Coaxial Stirling pulse tube cryocooler with active displacer

Mohammad Amin Abolghasemi[a,*], Hannah Rana[a], Richard Stone[a], Mike Dadd[a], Paul Bailey[a], Kun Liang[b]

[a]*Department of Engineering Science, University of Oxford, UK*
[b]*Department of Engineering and Design, University of Sussex, UK*

Abstract

Coaxial pulse tube cryocoolers are the configuration of choice as they allow better access to the cold head. Hence, a previously built and tested in-line pulse tube cryocooler which uses an active displacer for phase control has been modified into a coaxial configuration. The active displacer allows the mass flow and the pressure pulse at the cold end of the pulse tube to be easily adjusted for optimum performance. The displacer also allows the expansion power at the warm end of the pulse tube to be recovered in order to operate more efficiently. A numerical Sage model is used to demonstrate this by examining the work flows throughout the cryocooler and it is shown that more than 6% of the power required to drive the cryocooler comes from the warm end of the pulse tube via the displacer. When using an inertance tube or orifice, this expansion power is dissipated as heat which is why using a displacer can lead to a more efficient cryocooler. Moreover, the effect of changing the displacer phase and stroke on cryocooler performance and pressure characteristics is examined both experimentally and numerically.

Keywords: Stirling cycle, pulse tube, coaxial cryocooler, active displacer, phase optimisation

*Corresponding author
Email address: amin.abolghasemi@eng.ox.ac.uk (Mohammad Amin Abolghasemi)

Nomenclature

ΔP_{12}	Pressure drop across displacer; i.e. $P_1 - P_2$ (bar)
$\dot{m}$	Mass flow (g/s)
$\dot{W}_{\mathrm{in,c}}$	Linear compressor input power (W)
$\dot{W}_{\mathrm{in,d}}$	Displacer input power (W)
$\dot{W}_{\mathrm{in}}$	Total input power (W)
η_{r}	Relative Carnot efficiency
$\langle \dot{H} \rangle$	cyclic averaged enthalpy flow (W)
$\langle \dot{Q} \rangle$	cyclic averaged heat flow (W)
$\langle P\dot{V} \rangle_{\mathrm{c}}$	cyclic averaged compression space PV power (W)
$\langle P\dot{V} \rangle_{\mathrm{db}}$	cyclic averaged displacer back space PV power (W)
$\langle P\dot{V} \rangle_{\mathrm{df}}$	cyclic averaged displacer front space PV power (W)
ϕ_{d}	Phase angle between position of linear compressor and displacer
ϕ_{pm}	Phase angle between pressure pulse and mass flow at the cold end
$\phi_{P_{12}}$	Phase angle between P_1 and P_2
d_{d}	Displacer stroke (mm)
P_1	Pressure in the displacer back space (bar)
P_2	Pressure in the displacer front space (bar)
Q_{c}	Cooling power (W)
T_{c}	Cold end temperature (K)
T_{h}	Heat rejection temperature (K)

1. Introduction

Stirling pulse tube cryocoolers (SPTCs) are small refrigerators that provide cooling for detectors and other electronic devices to cryogenic temperatures. The SPTC is a hybrid cryocooler that combines the established technology of a Stirling cycle refrigerator with an incorporated pulse tube unit. The operation of an SPTC is governed by thermodynamic cycles using a working fluid, in this case helium, that results in an intricate interplay between the pressure pulse and mass flow at the cold end to achieve cooling [1]. It has been established that the pressure pulse at the cold end must lead the mass flow in phase in order to reduce regenerator losses [1]. Typically, in pulse tube cryocoolers, orifices and inertance tubes are used to achieve this [2, 3]. However, Shi et al. [4] highlights that the phase angle between pressure and mass flow is difficult to freely adjust using orifices and inertance tubes. Alternatively, expanders (also known as phase shifters) and displacers can be used to ensure the correct relationship between mass flow and pressure. These allow for the phase to be adjusted more easily and allow for a wider range of phase angles to be investigated.

The added benefit of a displacer (relative to an expander) is that it permits expansion power (PV power) to be recovered from the warm end of the pulse tube leading to a more efficient SPTC. Brito et al. [5] demonstrated the benefits in performance of a free warm end expander in pulse tube cryocooler and Zhu et al. [6] further presented a numerical design of an SPTC with a warm gas-driven displacer. In one of the earliest experimental studies, Shi et al. [4] demonstrated that the performance of a coaxial SPTC with a free moving displacer can help improve the efficiency of an SPTC by recovering the expansion power. SPTCs with displacers continue to be of interest as developers aim to increase the efficiency of their cryocoolers [7, 8, 9]. It is worth noting that although Stirling cryocoolers offer higher efficiencies in comparison to SPTCs, an SPTC with an ambient displacer is significantly less complicated to design and manufacture.

Displacers can be driven (i.e. active) or free moving (i.e. passive). SPTCs with active displacers present the further benefit of allowing for effortless fine-tuning of phase mid-operation for a more efficient cryocooler performance [10]. An active displacer is used in this study as it allows the optimum displacer phase and stroke values to be easily found while the SPTC is operating. This allows for a thorough experimental investigation of how the displacer dynamics affect the SPTC performance and the mass flow and

pressure in particular. This insight is extremely helpful when validating numerical models. Furthermore, once the optimum displacer dynamics are found, the spring stiffness and moving mass can be adjusted and the drive motor can be replaced with a suitable damper so that the active displacer is replaced by a passive one which operates at the optimum phase and stroke. In other words, the active displacer paves the way to an efficient passive displacer design. In comparison, designing a passive displacer from scratch with no starting point would require far more design iterations.

A coaxial configuration is used in this study to permit better access and integration of the SPTC cold head to focal plane assemblies and instrument surfaces, as reported by Wilson et al. [11] and Trollier et al. [12]. It also leads to a reduction in dead volume of the overall SPTC and thus Dang [13] refers to a coaxial configuration as the more compact choice for cryocooler integration. One of the challenges with a coaxial configuration is the difficulty in predicting the extent of fluid mixing at the cold head and the impact this has on the overall cooling performance [13, 14, 15]. It is therefore important to report on the experimental findings of coaxially configured SPTCs in order to better understand this and to validate numerical models. In this study, a relatively small cold head has been utilised for coaxial flow reversal. Previously, it was shown by Rana et al. that a Sage model [16] can be modified in order to correctly account for the coaxial flow inside an SPTC [15]. This study presents an experimental validation with Sage using this modelling method. Moreover, an enthalpy analysis was conducted to determine the work flow throughout the SPTC and to quantify the impact of recovering expansion power at the warm end of the pulse tube.

In summary, this paper reports firstly on the experimental findings of a coaxially configured SPTC with an active displacer. Secondly, experimental validation with a coaxial Sage model is presented. Finally, the validated Sage model is used to investigate the enthalpy flows within the SPTC, and to quantify the expansion power recovered.

2. Design and instrumentation

Fig. 1 shows a schematic of the coaxial SPTC along with the instrumentation used. The cryocooler consists of:

- A dual piston oil-free linear compressor which acts as a pressure wave generator with a typical operating frequency of 60 Hz (COMP in Fig. 1).
- An oil free single piston active displacer operating at the same frequency as the linear compressor (DISP). The active displacer is a moving coil loudspeaker motor design where 10 µm clearance seals around the displacer piston and shaft are maintained using flexure bearings. The design is very similar to the Oxford type clearance seal flexure bearing compressor design. For more detail on this design, the reader is referred to [17, 18]. In this paper the expansion space to the right of the displacer piston is referred to as the displacer front volume and the space to the left of the displacer piston is referred to as the displacer back volume.
- An annular heat rejector at ambient temperature filled with copper mesh, 60 wires per inch (HRJ).
- An annular regenerator filled with stainless steel mesh, 400 wires per inch (REG).
- A cold end heat exchanger (CHX). This was designed to also act as a flow straightener. The cold end temperature was recorded using a silicon diode cryogenic temperature sensor (expected accuracy $\pm 0.25\%$). A small heater and a PID temperature controller was used to maintain a user defined cold end temperature.
- A pulse tube (PT).
- A flow straightener at the warm end of the pulse tube filled with copper mesh, 60 wires per inch (FS).

The cold head assembly, consisting of the regenerator, the cold end heat exchanger and the pulse tube, was housed inside a vacuum chamber in order to minimise convective losses. A vacuum with pressures below 1×10^{-5} mbar (measured at the inlet to the vacuum system) was maintained throughout the

experiments. Aluminised Mylar radiation shields were also wrapped around the cold head assembly in order to minimise heat transfer via radiation, Fig. 2. The compressor and displacer motion were controlled via user defined sinusoidal waveforms using LabVIEW. These were amplified and then delivered to the components. The displacements were monitored using linear variable differential transformer (LVDT) displacement transducers. As well as the amplitude of the oscillations, the phase angle between the compressor and the displacer was recorded via a phase meter. By varying the active displacer motion relative to the linear compressor, the behaviour of the mass flow at the cold end can be altered. Moreover, pressure transducers were used to monitor the pressure either side of the active displacer. This data was recorded via the high speed data acquisition (HDAQ) card at a sampling rate of 5 kHz. Thermocouples were used to record component temperatures at a sampling rate of 10 Hz via the low speed data acquisition (LDAQ) card.

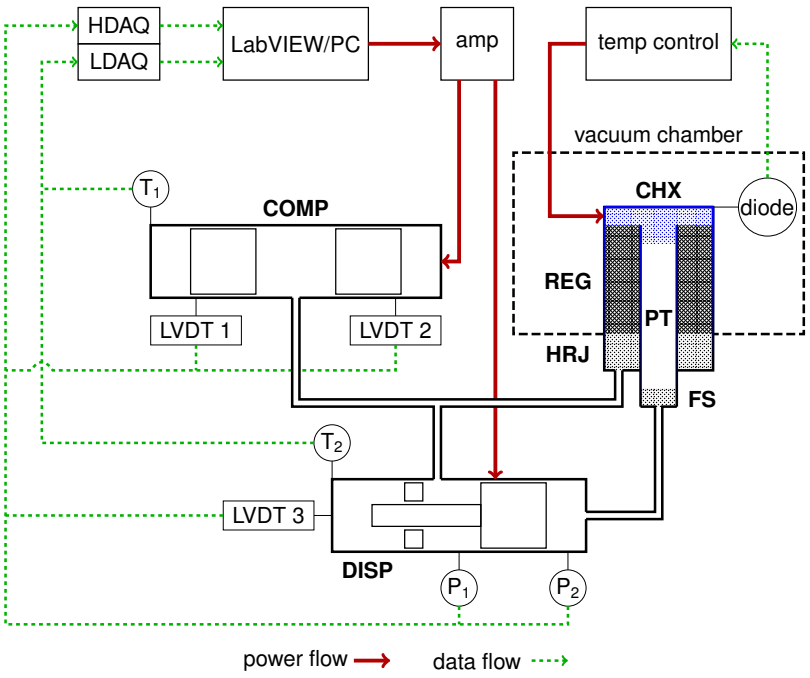

Figure 1: Coaxial SPTC experimental layout and instrumentation with abbreviations **COMP** for linear compressor, **DISP** for active displacer, **HRJ** for heat rejector, **REG** for regenerator, **PT** for pulse tube, **CHX** for cold end heat exchanger, **FS** for flow straightener, **amp** for amplifier, **HDAQ** for high speed data acquisition and **LDAQ** for low speed data acquisition, **T** for thermocouple and **P** for pressure transducer.

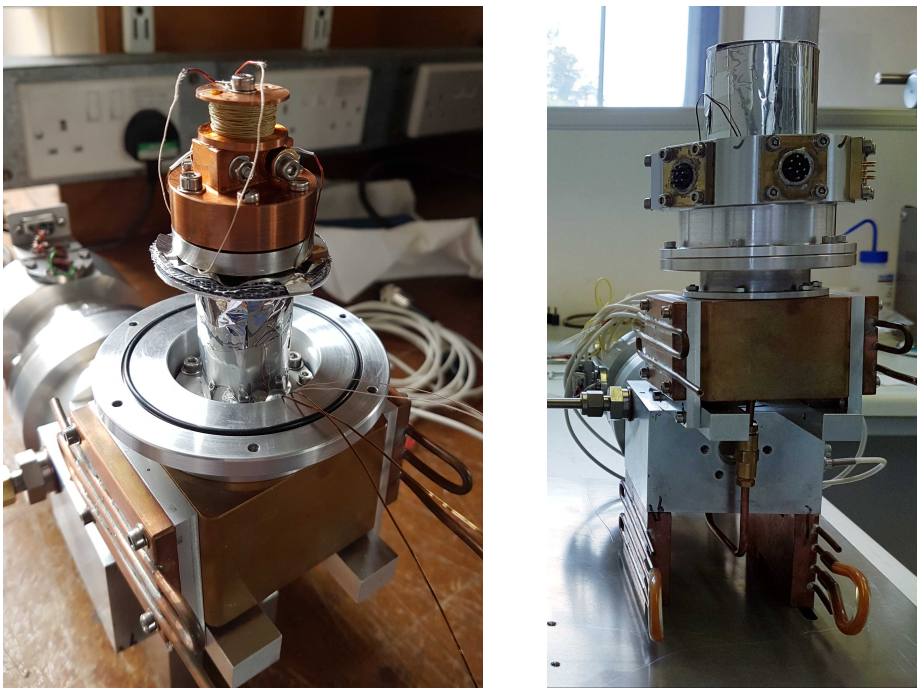

Figure 2: Photos of the coaxial SPTC showing (left) radiation shields around the regenerator, with the cold head exposed and (right) the lower half of the vacuum tank in place with radiation shields around the cold head.

3. Results

3.1. Cryocooler performance

In order to assess the SPTC performance sensitivity to the displacer motion, a number of tests were carried out at a fill pressure of 28 bar and with an operating frequency of 60 Hz. During these tests, the cold end was maintained at 80 K and the cooling power was recorded. Initially, a constant displacer stroke of 4 mm was used and the displacer phase (relative to compressor motion) was increased from 30° to 60°. Subsequently, a constant displacer phase of 45° was used and the displacer stroke was changed from 3.2 mm to 5.2 mm. A constant compressor stroke was used throughout, see Table. 1. The resulting cooling power and relative Carnot efficiency, η_r, along with predictions from Sage are shown in Fig. 3 where

$$\eta_\mathrm{r} = \frac{Q_\mathrm{c}}{\dot{W}_\mathrm{in}} \left(\frac{T_\mathrm{h}}{T_\mathrm{c}} - 1 \right) , \tag{1}$$

with

$$\dot{W}_\mathrm{in} = \dot{W}_\mathrm{in,c} + \dot{W}_\mathrm{in,d} . \tag{2}$$

Fill pressure	28 bar
Frequency	60 Hz
Compressor Stroke	8 mm
Displacer Stroke, d_d	3.2–5.2 mm
Displacer phase, ϕ_d	30–60°
Cold end temperature, T_c	80 K
Heat rejection temperature, T_h	300 K

Table 1: Performance sensitivity experimental test conditions.

The experimental results reveal optimum values for both displacer phase and stroke. The phase sensitivity plot suggests an optimum phase value of around $\phi_\mathrm{d} = 50°$ for maximum cooling power. Optimum efficiency occurs at a

lower value of $\phi_d = 45°$. In terms of displacer stroke, maximum cooling power occurs at $d_d = 4.5\,\text{mm}$ with maximum efficiency at $d_d = 4\,\text{mm}$. Noticeably, the peaks in both plots are broad and this suggests that a small deviation away from the optimum phase and stroke values will not have a significant effect on the SPTC performance.

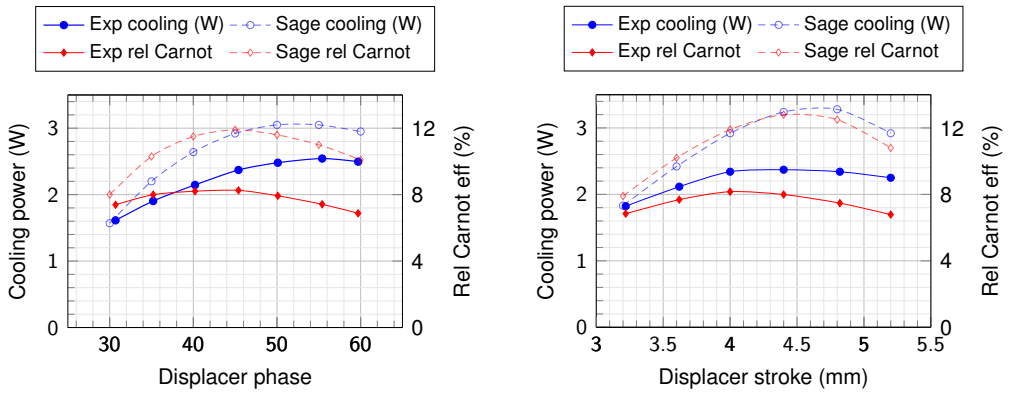

(a) Sensitivity to ϕ_d with $d_d = 4\,\text{mm}$

(b) Sensitivity to d_d with $\phi_d = 45°$

Figure 3: SPTC performance sensitivity to active displacer motion at an operating frequency of 60 Hz and 80 K with a constant compressor stroke.

Overall, the numerical Sage model captures the same trends as observed in the experimental results with the peaks occurring at the same displacer phase and stroke values as in the experiments. However, the Sage model generally predicts higher cooling powers and significantly higher efficiencies. The higher cooling powers in Sage occur because the numerical model underestimates the losses and heat transfer rates within the SPTC. The discrepancy is amplified in the efficiency values because on top of the differences in cooling power, for the Sage model there is no distinction between shaft power and input power whereas in reality not all of the input power is transferred into the compressor and displacer pistons. For the linear compressor the shaft power is around 80% of the input power (at 60Hz and 28bar), but the displacer is not very efficient at these operating conditions with a motor efficiency below 50%. This is because the displacer is operating away from its optimum operating frequency, but this is not a significant loss since the displacer input power is a small fraction of the total input power as shown in Fig. 4. Having said that, at the higher displacer phase and stroke values, the displacer input power increases and it becomes a greater fraction

of the total input power.

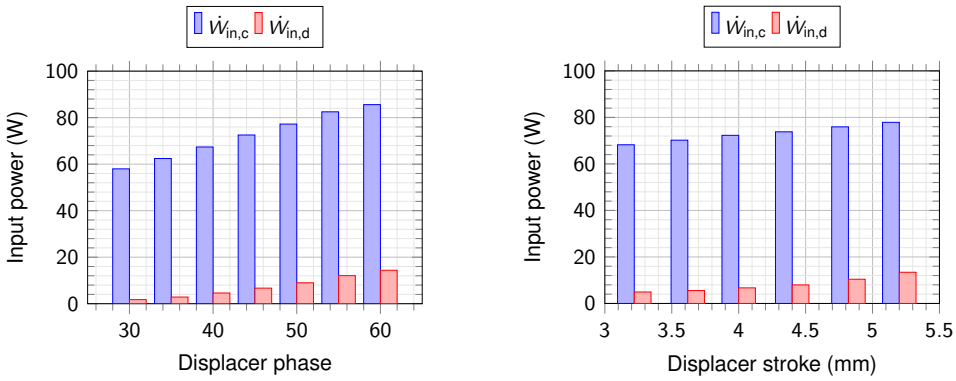

(a) Sensitivity to ϕ_d with $d_d = 4\,\text{mm}$

(b) Sensitivity to d_d with $\phi_d = 45°$

Figure 4: Compressor ($\dot{W}_{in,c}$) and active displacer ($\dot{W}_{in,d}$) contributions to total input power during the displacer phase and stroke sensitivity experiments.

3.2. Pressure pulses and mass flows

The pressure transducers either side of the displacer piston allow for a closer examination of how the displacer motion affects the pressure pulse within the SPTC. Fig. 5 shows the peak-to-peak pressure values recorded during the experiments, as well as the drop in peak-to-peak pressure and change in pressure phase across the displacer.

Based on the results shown, when varying the displacer phase, P_1 is almost unaffected but P_2 drops with the peak-to-peak value reducing by almost 25% during a 30° change in displacer phase. Hence, the pressure drop across the displacer increases significantly from 1.2 bar to 2.1 bar. However, despite this reduction in peak-to-peak pressure, the phase angle between the pressure pulses either side of the displacer remains almost constant at around 6°.

On the other hand, when varying the displacer stroke, both P_1 and P_2 slightly increase and there is only a small increase in pressure drop across the displacer from 1.5 bar to 1.8 bar even though the displacer stroke has almost doubled. Furthermore, although changing the displacer phase did not affect the pressure phase, varying the displacer stroke leads to a variation in the pressure phase of more than 13°.

The results from the Sage model are also shown in Fig. 5 alongside the experimental results. The peak-to-peak values are slightly higher in Sage,

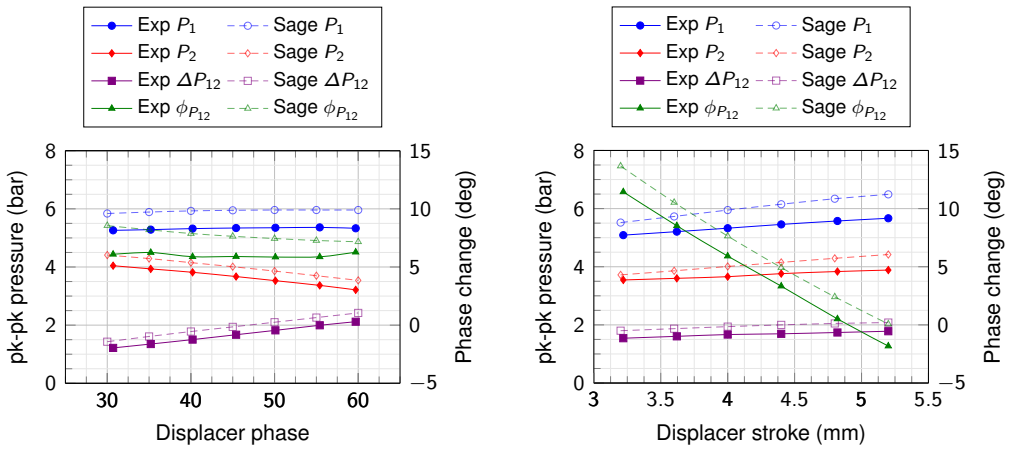

(a) Sensitivity to ϕ_d with $d_\mathrm{d} = 4\,\mathrm{mm}$

(b) Sensitivity to d_d with $\phi_\mathrm{d} = 45°$

Figure 5: Pressure pulse peak-to-peak and phase change across the displacer as a result of varying the displacer phase and stroke.

but once again the numerical results display the same trends as observed in the experiments. This gives confidence in the validity of the Sage predictions and this is important because now the Sage model can be used to dissect what is happening at the cold end of the SPTC.

As mentioned previously, the performance of the SPTC is dominated by the relationship between the mass flow and the pressure pulse at the cold end. Fig. 6 shows the variation in peak-to-peak mass flow and the mass flow phase angle relative to the pressure pulse at the cold end as predicted in Sage. Increasing the displacer phase leads to an increase in peak-to-peak mass flow from 2.5 g/s to 4.3 g/s and similarly increasing the displacer stroke results in a 1.4 g/s increase. Conversely, the mass flow phase relative to pressure behaves very differently in the two tests. A 30° increase in displacer phase leads to a 9° reduction in ϕ_pm whereas a 2 mm increase in displacer stroke leads to a 33° increase.

The cooling power depends on the magnitude of the mass flow and pressure in the cold head and their phase relationship. Based on Fig. 6, the phase difference between pressure and mass flow at optimum operating conditions of $\phi_\mathrm{d} = 45°$ and $d_\mathrm{d} = 4\,\mathrm{mm}$ is around 20°. Variations in displacer phase and stroke away from $\phi_\mathrm{d} = 45°$ and $d_\mathrm{d} = 4\,\mathrm{mm}$ result in a change in ϕ_pm away from its optimum value. With regards to the pressure in the cold head, it is safe to assume that this pressure is not too different to that at

the front of the displacer, i.e. P_2, since most of the pressure drop occurs across the regenerator. With increasing displacer phase, this peak-to-peak pressure is dropping while it remains constant with increasing displacer stroke (see Fig. 5). Conversely, the mass flow amplitude increases with increasing displacer phase and stroke. It is the combination of these three variations that leads to the change in SPTC cooling power observed in Fig. 3.

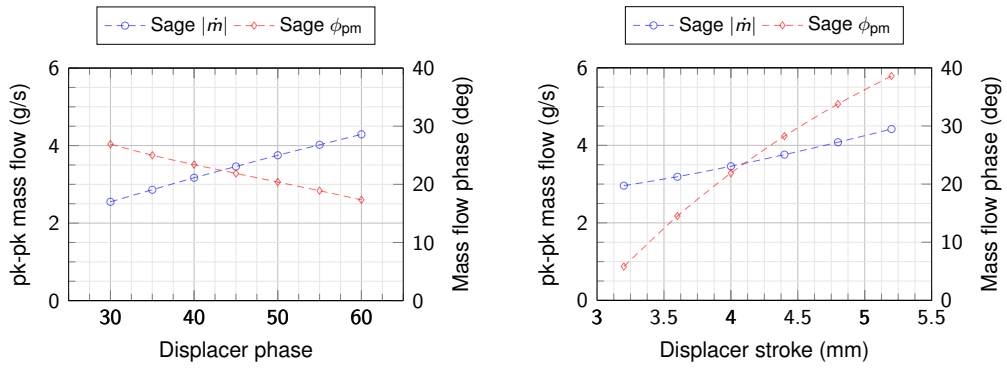

(a) Sensitivity to ϕ_d with $d_d = 4\,\text{mm}$ (b) Sensitivity to d_d with $\phi_d = 45°$

Figure 6: Variation in mass flow peak-to-peak and phase (relative to pressure) for different displacer phase and stroke values according to the Sage model.

3.3. Work flows

The Sage model also allows for an in depth look into the work flows within the SPTC. The cyclic average enthalpy flows along with the heat transfers into or out of each component is shown in Fig. 7. The PV powers into or out of the compression space, the displacer front and back spaces are also shown. The values shown are for the optimum operating conditions where $\phi_d = 45°$ and $d_d = 4\,\text{mm}$. This work flow demonstrate the ability of the displacer to recycle the expansion work from the warm end of the pulse tube. According to Sage, out of the 69 W of enthalpy flowing into the heat rejector (which is essentially driving the cryocooler), 4.5 W is coming from the displacer. It was previously shown that the Sage model performance and pressure values follow the same trends as in the experiments and therefore the work flow shown can be treated as a qualitative representation of the work flow in the real system.

Note that in the ideal case there would be no enthalpy flow down the regenerator and the pulse tube would deliver all of the enthalpy received

from the cold head to the displacer front space. However, based on the Sage model, the regenerator transfers 3.5 W of enthalpy from its warm end to the cold head and less than 80% of the 7 W of enthalpy from the cold head is delivered to the displacer. In the real SPTC this is likely to be even less since the heat transfer is almost certainly underestimated in the Sage model. Bear in mind that in the real system the connection from the the flow straightener into the displacer is via a copper tube with ambient air on the outside.

Moreover, the flow straightener is acting as a heat exchanger and ideally one would not want any of the expansion power to be rejected as heat, but it is difficult to isolate the flow straightener given its proximity to the heat rejector. Figure 8 shows how the heat lost through the warm end flow straightener, $\langle \dot{Q} \rangle_{\mathrm{FS}}$, compares with the enthalpy recycled back into the system, $\langle \dot{H} \rangle_{\mathrm{FS}}$, as a function of the displacer phase and stroke. This highlights the benefit of using a displacer instead of an inertance tube where no enthalpy would be recovered and all would be lost as heat. As the displacer phase is increased, a relatively constant amount of heat is lost from the

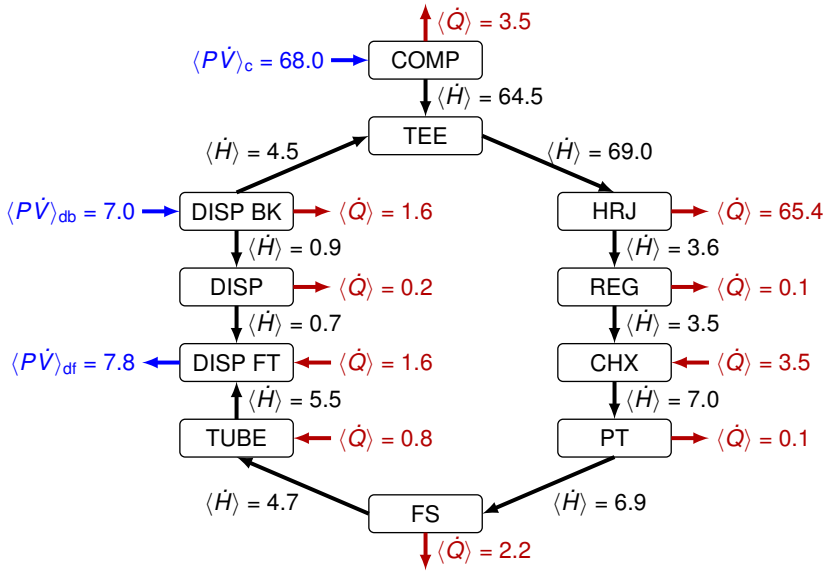

Figure 7: Cyclic averaged enthalpy flows (black), PV powers (blue) and heat flows (red) according to Sage in units of W. Abbreviations are the same as those described in Fig. 1 plus **DISP FT** and **DISP BK** for displacer front and back volumes, respectively. Also, **TEE** is the T junction where the output from the displacer is connected back into the cycle. Results shown are for the optimum operating conditions with $\phi_{\mathrm{d}} = 45°$ and $d_{\mathrm{d}} = 4\,\mathrm{mm}$.

system, whereas an increase in enthalpy transferred to the back end of the displacer is observed. This implies that with an increase in displacer phase, the warm end flow straightener functions more effectively. The inverse can be observed with an increase in displacer stroke. A greater amount of heat is lost as the displacer stroke is increased, and the enthalpy recycled back into the displacer back end is relatively constant. It is worth noting that this data presents the cyclic-averaged enthalpy and heat flows; hence, with an increase in displacer stroke, the volume of gas being acted on is larger whereas it remains constant as the displacer phase is altered.

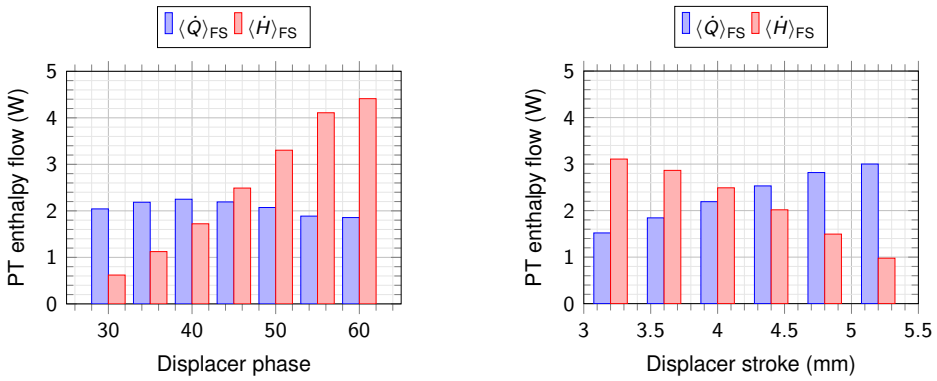

(a) Sensitivity to ϕ_d with $d_d = 4\,\text{mm}$

(b) Sensitivity to d_d with $\phi_d = 45°$

Figure 8: Proportions of pulse tube enthalpy flow which is lost as heat $\langle\dot{Q}\rangle_{FS}$ alongside that which is delivered to the displacer $\langle\dot{H}\rangle_{FS}$ according to the Sage model.

3.4. PV powers

The PV powers are also of interest because although the enthalpy flows of the real system are not available, PV powers can be computed using the experimental pressure measurements and the LVDT displacement data. Figure 9 shows the experimental PV plots for the compression space and the displacer front and back spaces. The plot shown corresponds to the optimum operating conditions of $\phi_d = 45°$ and $d_d = 4\,\text{mm}$. In order to generate this, it is assumed that the pressure in the compression space and in the displacer back space are the same and equal to P_1. These two volumes are connected via a 130 mm long tube and since the pressure drop across this tube is negligible compared to that across the cold head assembly (dominated by the regenerator), this is a reasonable assumption. According

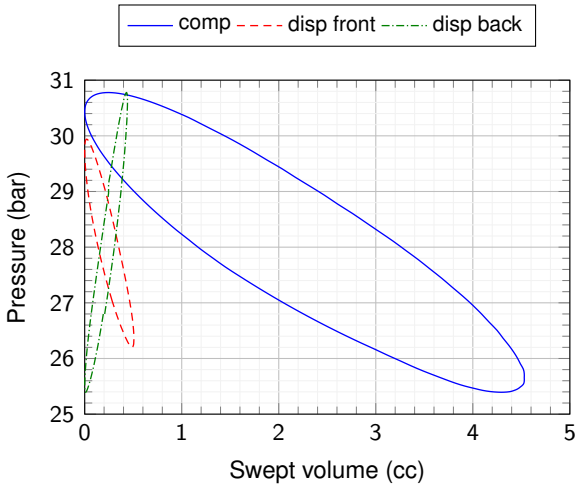

Figure 9: Experimental PV plot at the optimum operating conditions with $\phi_\mathrm{d} = 45°$ and $d_\mathrm{d} = 4\,\mathrm{mm}$ where $\langle P\dot{V}\rangle_\mathrm{c} = 51.8\,\mathrm{W}$, $\langle P\dot{V}\rangle_\mathrm{df} = 3.7\,\mathrm{W}$ and $\langle P\dot{V}\rangle_\mathrm{db} = 3.7\,\mathrm{W}$.

to the experimental data, the PV powers are 51.8 W in the compression space and 3.7 W in both the displacer front and back spaces. These values are smaller than those predicted by Sage (see Fig. 7), but the proportions of recycled $\langle P\dot{V}\rangle_\mathrm{db}$ to compressor input $\langle P\dot{V}\rangle_\mathrm{c}$ are in good agreement with the Sage model predicting 10% and the experimental data indicating 7%.

Fig. 10 shows the variation in compressor and displacer PV powers as the displacer phase and stroke were changed. Both experimental and Sage results are shown with the Sage results once again following the same trends as the experimental data. The PV power into the compression and displacer back space both rise with increasing displacer phase and stroke. However, the extracted PV power from the displacer front space does not rise as sharply when increasing the displacer phase and remains almost constant when varying the displacer stroke.

In future, the active displacer will be replaced by a passive one. In order for the displacer to operate passively, the extracted PV power from the front space must match the PV power going into the back space. In reality the extracted PV power must be slightly larger in order to overcome friction but since there is a relatively large clearance between the displacer piston and the surrounding cylinder, the frictional losses will be relatively small. Hence, at the point where $\langle P\dot{V}\rangle_\mathrm{df}$ and $\langle P\dot{V}\rangle_\mathrm{db}$ cross, the displacer is operating almost passively. When $\langle P\dot{V}\rangle_\mathrm{db}$ is greater than $\langle P\dot{V}\rangle_\mathrm{df}$, the

additional power is provided by the active displacer motor and when $\langle P\dot{V}\rangle_{\mathrm{db}}$ is smaller than $\langle P\dot{V}\rangle_{\mathrm{df}}$, the active displacer is acting as a damper. Now that the optimum displacer phase and stroke has been established to be $\phi_{\mathrm{d}} = 45°$ and $d_{\mathrm{d}} = 4\,\mathrm{mm}$, the displacer moving mass and spring stiffness can be manipulated such that it can operate passively at this optimum operating point.

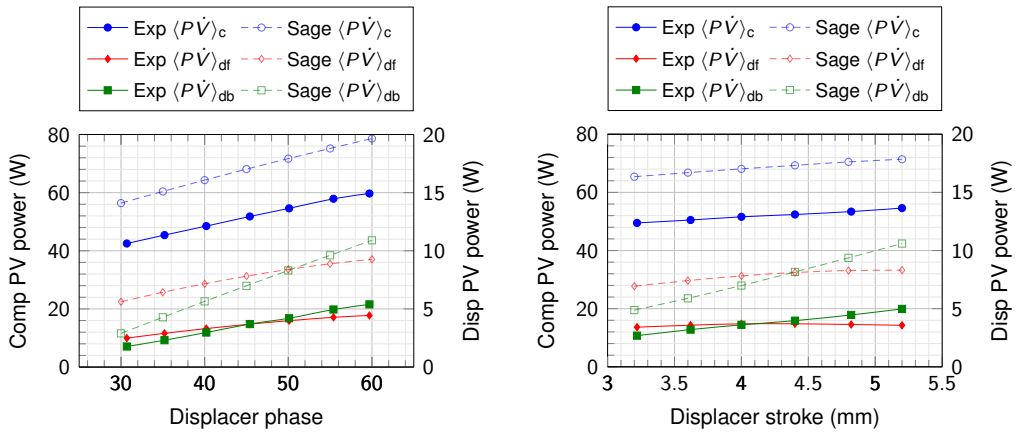

(a) Sensitivity to ϕ_{d} with $d_{\mathrm{d}} = 4\,\mathrm{mm}$

(b) Sensitivity to d_{d} with $\phi_{\mathrm{d}} = 45°$

Figure 10: Compressor and displacer PV power sensitivity to active displacer motion.

4. Conclusions

A coaxial SPTC with an active displacer has been successfully built and tested. In summary:

1. The active displacer allows the performance of the SPTC to be easily optimised during operation by varying the behaviour of the mass flow and pressure pulse at the cold end. This is achieved by varying the displacer motion relative to the compressor.
2. Operating at optimal phase, the cryocooler produces 2.4 W of cooling power at 80 K with an input power of 79 W. This corresponds to a relative Carnot efficiency of 8.3%.
3. The displacer is able to recycle some of the expansion power from the warm end of the pulse tube back into the cycle and it is shown that 6% of the power required to drive the cryocooler comes from the

displacer. This can help produce a more efficient SPTC compared to the commonly used inertance tube SPTC.

4. Although the trends are predicted correctly, the current numerical Sage model overestimates the cooling power and relative Carnot efficiency due to limitations in modelling 3D flow effects. A better understanding of the 3D flow within the SPTC can help further improve the Sage model.

Future plans include replacing the active displacer with a passive equivalent with the correct moving mass and spring stiffness in order to operate at the optimum displacer phase and stroke values. This will further improve the cryocooler performance as no power will be required to drive the displacer. Furthermore, CFD modelling will be used to further refine the flow within the SPTC, especially within the pulse tube, in order to improve the SPTC performance by reducing losses due to flow mixing.

Acknowledgement

The authors acknowledge the support of Honeywell Hymatic during the design and manufacture of the SPTC. The authors further acknowledge support from the EPSRC under research project EP/N017013/1.

References

[1] R. Radebaugh, Development of the pulse tube refrigerator as an efficient and reliable cryocooler, Proc. Institute of Refrigeration (London) (2000).

[2] P. Kittel, Ideal orifice pulse tube refrigerator performance, Cryogenics 32 (9) (1992) 843–844. doi:10.1016/0011-2275(92)90320-A.

[3] P. De Boer, Performance of the inertance pulse tube, Cryogenics 42 (3) (2002) 209–221. doi:10.1016/S0011-2275(02)00007-3.

[4] Y. Shi, S. Zhu, Experimental investigation of pulse tube refrigerator with displacer, International Journal of Refrigeration 76 (2017) 1–6. doi:10.1016/j.ijrefrig.2017.01.022.

[5] M. Brito, G. Peskett, Experimental analysis of free warm expander pulse tube, Cryogenics 41 (10) (2001) 757–762. doi:10.1016/S0011-2275(01)00160-6.

[6] S. Zhu, M. Nogawa, Pulse tube stirling machine with warm gas-driven displacer, Cryogenics 50 (5) (2010) 320–330. doi:10.1016/j.cryogenics.2010.01.011.

[7] X. Wang, Y. Zhang, H. Li, W. Dai, S. Chen, G. Lei, E. Luo, A high efficiency hybrid stirling-pulse tube cryocooler, Aip Advances 5 (3) (2015) 037127. doi:10.1063/1.4915900.

[8] M. Wang, H. Xu, Y. Lin, Z. Zhang, S. Zhu, Experimental investigation of pulse tube refrigerator with rod type displacer as phase shifter, International Journal of Refrigeration 93 (2018) 47–51. doi:10.1016/j.ijrefrig.2018.06.006.

[9] A. de Waele, Pulse-tube refrigerator with a warm displacer: Theoretical treatment in the harmonic approximation, Cryogenics 100 (2019) 53–61. doi:10.1016/j.cryogenics.2019.04.002.

[10] M. A. Abolghasemi, K. Liang, R. Stone, M. Dadd, P. Bailey, Stirling pulse tube cryocooler using an active displacer, Cryogenics 96 (2018) 53 – 61. doi:10.1016/j.cryogenics.2018.10.004.

[11] K. B. Wilson, C. C. Fralick, D. Gedeon, M. Yoshida, S. Kawahara, Sunpower's CPT60 pulse tube cryocooler, Cryocoolers 14 (2007) 123–132.

[12] T. Trollier, J. Tanchon, J. Buquet, A. Ravex, Status of Air Liquide space pulse tube cryocoolers, Cryocoolers 15 (2009) 115–123.

[13] H. Dang, High-capacity 60 K single-stage coaxial pulse tube cryocoolers, Cryogenics 52 (4-6) (2012) 205–211. doi:10.1016/j.cryogenics.2012.01.006.

[14] H. Dang, L. Wang, Y. Wu, SITP's Miniature Coaxial Pulse Tube Cryocooler, Cryocoolers 16 (2011) 103–110.

[15] H. Rana, M. A. Abolghasemi, R. Stone, M. Dadd, P. Bailey, Numerical modelling of a coaxial Stirling pulse tube cryocooler with an active displacer for space applications, Cryogenics 106 (2020) 103048. doi:10.1016/j.cryogenics.2020.103048.

[16] D. Gedeon, Sage: Object-Oriented Software for Cryocooler Design, Cryocoolers 8 (1995) 281–292.

[17] P. Bailey, M. Dadd, R. Stone, High Speed Compressors, Cryocoolers 17 (2012) 347–356.

[18] K. Liang, M. Dadd, P. Bailey, Clearance seal compressors with linear motor drives. Part 1: Background and system analysis, Proceedings of the Institution of Mechanical Engineers, Part A: Journal of Power and Energy 227 (3) (2013) 242–251. doi:10.1177/0957650913475619.